Chapter 7
Madden Julian Oscillation

7.1 Observational Aspects

The Madden Julian Oscillation, often abbreviated as MJO, is a major feature of the tropical circulation. It manifests as quasi-periodic fluctuations in the sea level pressure and wind structure, and consequently – in the sea surface temperature, convection and rainfall. The time scale of the phenomenon is, on average, about 30–60 days. It was first discovered by Madden and Julian (1971) as they studied the zonal winds and the sea level pressure in a 10-year long record of tropical data. The MJO time scales carry a significant proportion of the atmospheric variance in the tropics.

In order to see this phenomenon clearly, a band pass filter in time is usually applied. Once the filtering is done, the MJO sea level pressure anomaly manifests as a planetary wave that moves from west to east, completing a full circle around the globe in about 40 days. The largest anomaly (roughly a few mb) are found in the equatorial latitudes, particularly over the equatorial Indian Ocean and the equatorial western Pacific Ocean. The seasonal and geographical distributions of the 850 mb zonal wind anomalies associated with the MJO are shown in Fig. 7.1a–d. Some of the prominent features seen here are the build-up of the zonal wind anomalies over the near-equatorial latitudes during the spring and summer seasons of the northern hemisphere. During these two seasons, large anomalies reside over the Arabian Sea and extend eastwards. The values during summer (the summer monsoon season) are as large as 3–5 ms^{-1}. These values are sufficiently large that one can in fact see the presence of this eastward propagating MJO wave in such wind field data sets.

By the fall season the Indian and Pacific Ocean amplitudes of the zonal wind anomalies on the MJO time scale cover a smaller area. During the winter months most of the tropics carry weaker amplitudes, on the order of 1–2 ms^{-1}. The MJO in the tropics stands out because it carries a sizable proportion of the total variance of the wind field. It is interesting to note that some of the largest amplitudes of oscillation of the zonal wind on the time scale of 20–60 days reside polewards of the 50° latitudes. Here the amplitude reaches as high as 9 ms^{-1}, mostly over the oceanic regions.

T.N. Krishnamurti et al., *Tropical Meteorology: An Introduction*,
Springer Atmospheric Sciences, DOI 10.1007/978-1-4614-7409-8_7,

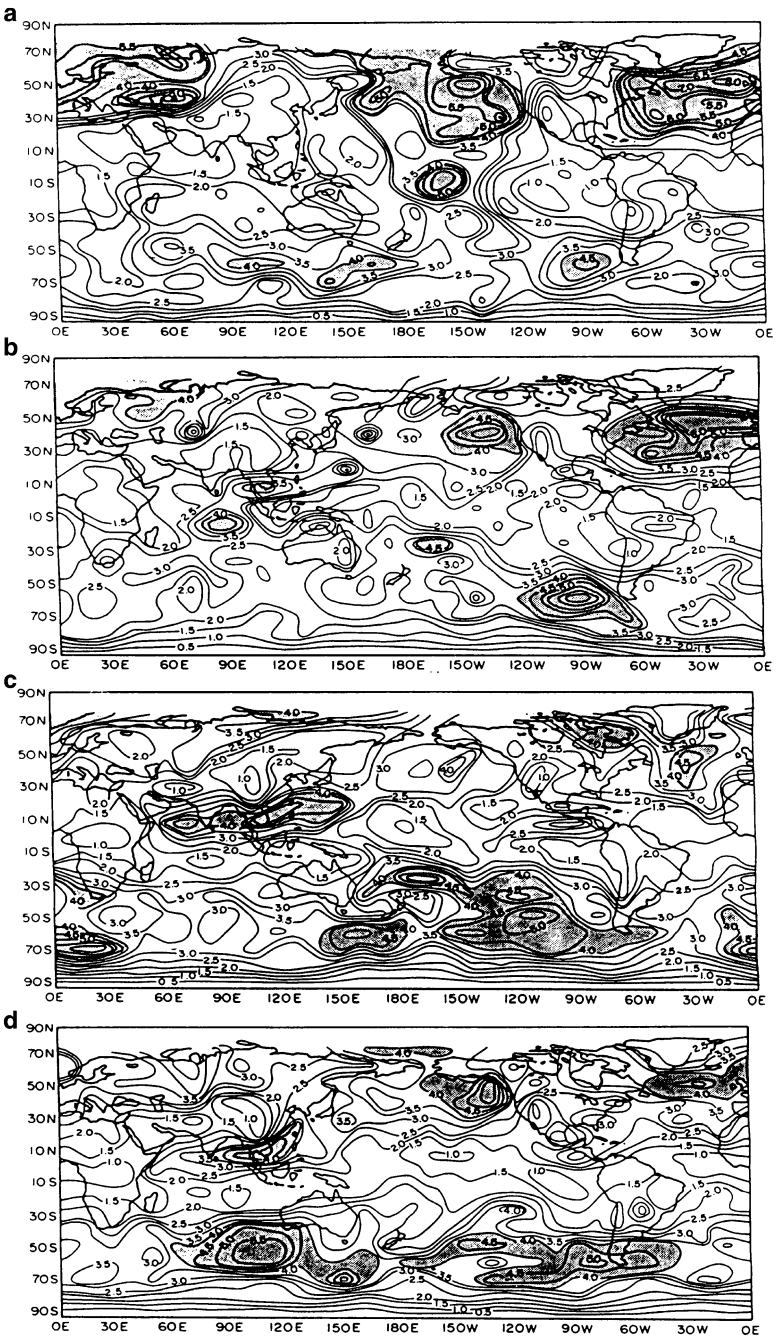

Fig. 7.1 Maximum zonal wind at 850 mb of frequency filtered motions during individual seasons (ms^{-1}) (**a**) winter, (**b**) spring, (**c**) summer and (**d**) fall (After Krishnamurti et al. 1992a)

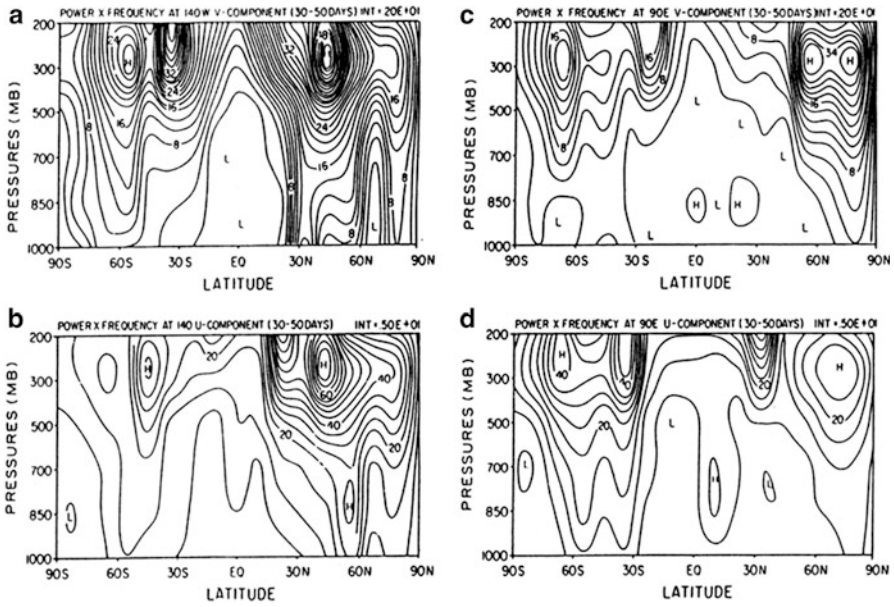

Fig. 7.2 Vertical distribution of power spectra (power times frequency) analyzed as function of latitude and pressure for the following variables: (**a**) v component at 140°W, (**b**) u component at 140°W, (**c**) v component at 90°E, (**d**) u component at 90°E (After Krishnamurti et al. 1992a)

This mid-latitude/polar feature however is not called the MJO. Over the high latitudes – in the region of the Icelandic and Aleutian lows of the northern hemisphere, and polewards of the roaring 40 s of the southern hemisphere – the MJO time scale oscillation contributes less to the total variance. Here the dominant time scale is around 4–6 days. If one looks at the vertical structure of the power spectra of the MJO time scale we note that the largest power again resides in these high latitudes of the polar region (Fig. 7.2). Here we show a plot of the power spectra (power times frequency) plotted for different latitudes and pressure levels. In this illustration we show the power spectra for the meridional and zonal components of the winds at 140°W (eastern Pacific) and 90°E (Monsoon) regions. Most of the large power can be seen polewards of 40° latitude over the upper troposphere. At 90°E one can see the large power of the zonal wind near 850 mb reflecting the Monsoonal modulation on the time scale of the MJO. These results are based on year long data sets and show the importance of this time scale for the monsoon.

The MJO wave is baroclinic in the tropical latitudes and is quasibarotropic over the higher latitudes. This is best seen from the vertical structure of the phase of the MJO wave. Figure 7.3 illustrates the amplitude of the zonal wind from an year-long data set for two tropical sites (left) and two polar sites (right). The phase of the zonal wind (westerlies are shaded, easterlies are unshaded) shows a clear reversal from the lower to the upper troposphere. Such change of phase is absent over the higher latitudes. This is what we mean by the more baroclinic structure for the MJO time

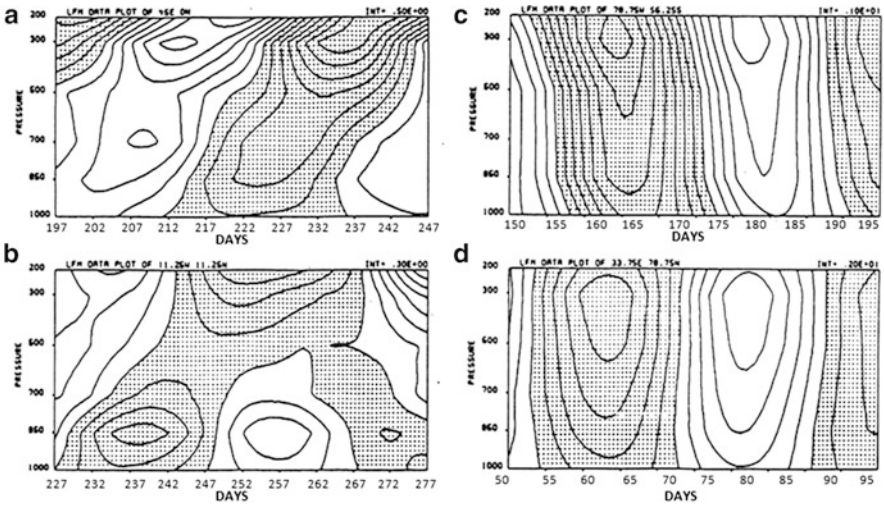

Fig. 7.3 Pressure–time analysis of the zonal wind on the time scale of 30–50 days for two tropical grid points (**a**) and (**b**) and for two higher latitude points (**c**) and (**d**). The units are ms^{-1}. Shaded area denotes negative values. The interval of analysis is shown on the top right of each panel (After Krishnamurti et al. 1992a)

scale over the tropics and a more barotropic structure in the extratropics. The MJO is intimately connected to organized tropical convection that prefers a lower pressure in the lower troposphere and a higher pressure aloft. Over the higher latitudes this time scale may be more dynamically driven.

The globally eastward propagating MJO wave over the tropics is a divergent wave. It carries convergence or divergence over one half of the wave as it progresses eastwards. This can be seen from the velocity potential maps. The velocity potential χ is defined from the equation

$$\nabla^2\chi = -\nabla\cdot\vec{\mathbf{V}} = -\nabla\cdot\vec{\mathbf{V}}_\chi, \tag{7.1}$$

where the divergent component of the wind is $\vec{\mathbf{V}}_\chi = -\nabla\chi$ and $\vec{\mathbf{V}}$ is the total wind. To map the field of χ one needs to first perform an analysis of the wind field $\vec{\mathbf{V}}$. Figure 7.4 illustrates a sequence of charts at intervals of every 5 days that shows the zonal passage of the MJO wave. This wave during 1979 traversed around the globe in roughly 30 days. These are the velocity potential charts that were obtained from local time filtering of the wind (u,v) at each grid location first and the divergence $-\nabla^2\chi$ computed next. The field of χ is obtained from a solution of the Poisson equation $\nabla^2\chi = -\nabla\cdot\vec{\mathbf{V}}$. This MJO wave is a long wave with most of its variance in the zonal wave numbers 1 and 2. Half of this wave carries low values of χ and the other half carries high values. That implies in fact that the wave has alternating features of divergence and convergence. The tropical weather seems to be modulated by the passage of these waves, i.e. a convergent part of the wave in the lower troposphere favors weather activity and vice versa.

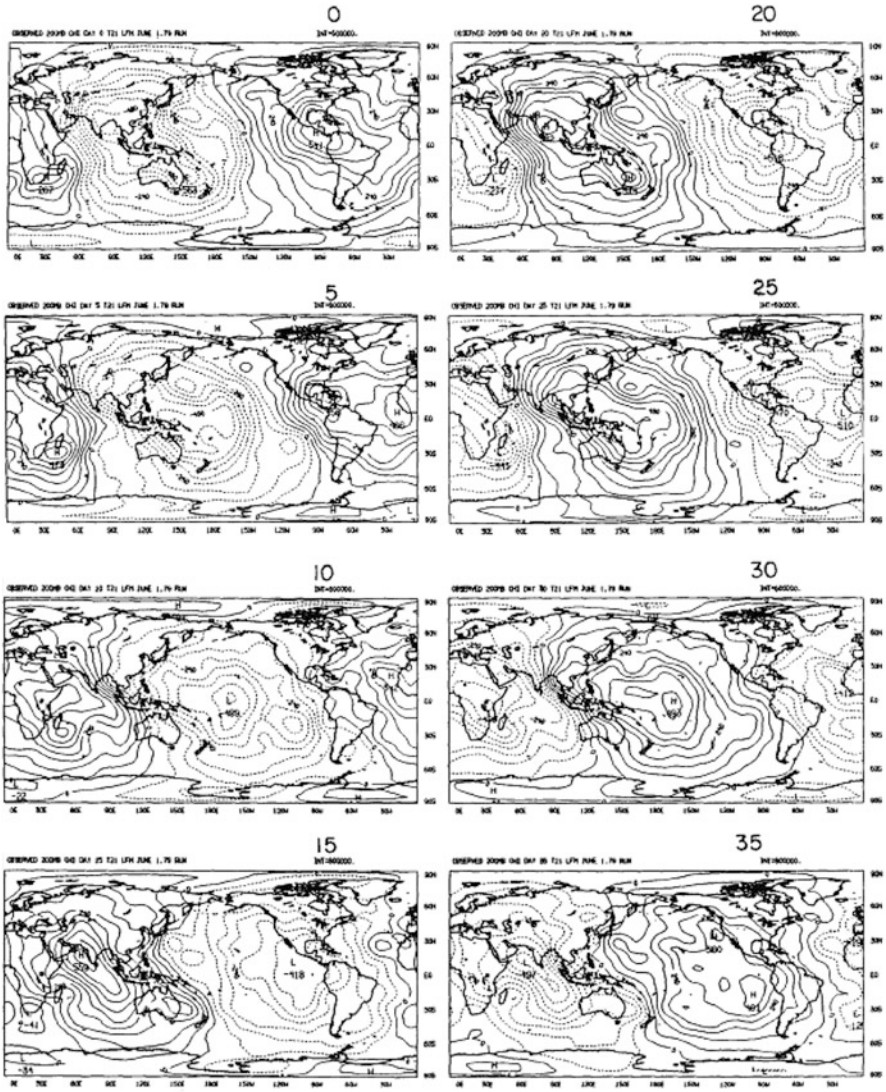

Fig. 7.4 Panels of the velocity potential at 200 mb based on observed wind. Interval of isopleths 60×10^{-6} $m^2 s^{-1}$. Day 0 is 1 June 1979. Maps are shown at intervals of 5 days. After Krishnamurti et al. (1992b)

The eastward propagation of the MJO wave can be illustrated with a Hovmüller diagram of the velocity potential (Fig. 7.5). Here the longitudes are shown along the abscissa and the ordinate denotes time for an entire year. The time-filtered velocity potential χ on the time scale of the MJO averaged between 5°S and 5°N is illustrated here. Here we see this spectacular phenomenon of MJO. These waves for nearly

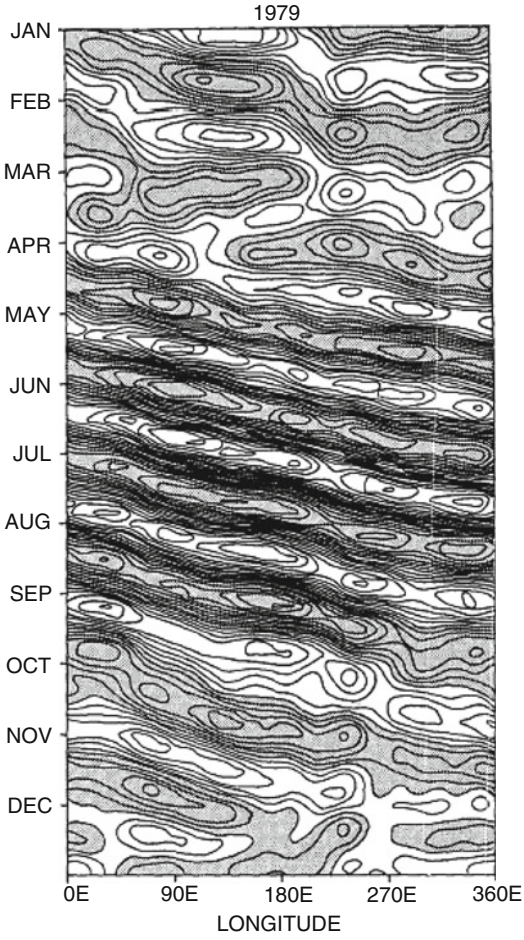

Fig. 7.5 An x-t diagram of the 200 mb velocity potential during the FGGE year. This represents an average from 50S to 50N. The contour interval is $1.3 \times 10^6 m^2 s^{-1}$ (After Krishnamurti et al. 1985)

the entire year propagate around the Earth on a time scale of roughly 40 days. The amplitudes of the waves are largest between April and October. The largest amplitudes are seen over the Asian and west Pacific Ocean longitudes. As stated before, the passage of an upper air divergence seems to modulate the weather as this slow moving wave goes by.

That modulation of weather was illustrated by Nakazawa (1988). He showed that an envelope of this MJO wave carries within it (over regions of lower tropospheric convergence) considerable meso-convective precipitating cloud elements. Those individual elements are seen clearly to move westwards and the entire envelope moves eastwards. The cloud elements normally move westward at a speed of roughly 5–10° longitude/day, whereas the envelope moves eastward at a rate of roughly 10° longitude/day. These two time scales clearly carry some interesting scale interactions that will be discussed in Chap. 8.

There is a monsoonal anomaly in this zonal propagation that is evident if we look at latitudes between 5°N and 30°N over Asia. While the near-equatorial wave on the MJO time scale moves eastward, the off-equatorial wave over Asia seems to carry a meridionally propagating component. This off-equatorial component of the MJO wave is not simply propagating eastwards. There is a meridional propagation of a wave that is called "intraseasonal oscillation", or ISO. This has a meridional wave length of roughly 3,000 km and propagates at a speed of about 1° latitude/day. It carries again alternating phases of divergence and convergence in the lower troposphere, carrying disturbed and undisturbed weather respectively. This meridionally moving feature is on the same time scale as the MJO. It appears to be a reflected Rossby gravity wave, i.e. the equatorial Kelvin wave (the eastward propagating MJO) being reflected by the Sumatra mountains. That has not been proven but deserves to be examined. This meridionally propagating intraseasonal oscillation called the monsoonal ISO is a divergent wave. The meridional passage of winds, especially at the 850 mb level, can illustrate this wave from time filtered data sets (Fig. 7.6). Those are troughs and ridges of waves that alternately pass northward from the equatorial latitudes. This figure illustrates roughly one cycle of this major phenomenon. The point to note here is that the summer monsoon climatology at 850 mb that carries the trade wind easterlies, the cross equatorial flow offshore from Kenya, the Somali jet east of the Horn of Africa (near Somalia) and the southwesterly monsoonal flow over the central Arabian Sea is modulated by the passage of the ISO wave northwards over South Asia and South East Asia. This passage of the ISO waves tends to strengthen or weaken the southwest monsoon current over the Arabian Sea. These are called parallel and antiparallel flows with respect to climatology. The modulation of monsoon weather by the passage of ISO waves depends on the strengthening (parallel) or weakening (antiparallel) of the climatological southwesterly monsoon. One can also carry out band pass filtering of rainfall data or of the OLR data as a proxy for clouds and see the passage of weather that is a part of the ISO waves. The variables where this feature is most conspicuous include: specific humidity, precipitation, total winds, clouds, and divergence.

Several studies have been carried out on the place of origin of these ISO waves. The seat of origin seems to be the southern equatorial trough near 5°S. That is a pressure trough – a clockwise wind near 5°S, best seen in the climatology of the lower troposphere during the summer months. A July climatology of low level winds is shown in Fig. 7.7 where the southern equatorial trough can be readily seen. To illustrate the meridional passage of this regime one can show latitude/time plots of variables such as the zonal wind and the relative vorticity at the 850 mb level during selected weeks of ISO passage. Those are illustrated in Fig. 7.8a, b. Here the time filtered data on the time scale of MJO/ISO for the zonal wind and the relative vorticity are shown at the 850 mb level. We clearly see the origin of the ISO waves near 0–5°S latitudes. The waves move northward carrying alternating components of westerlies and easterlies (amplitude about 3 ms^{-1}) and of cyclonic and anticyclonic vorticity (amplitude about 0.5×10^{-5} s^{-1}). Additionally, we note

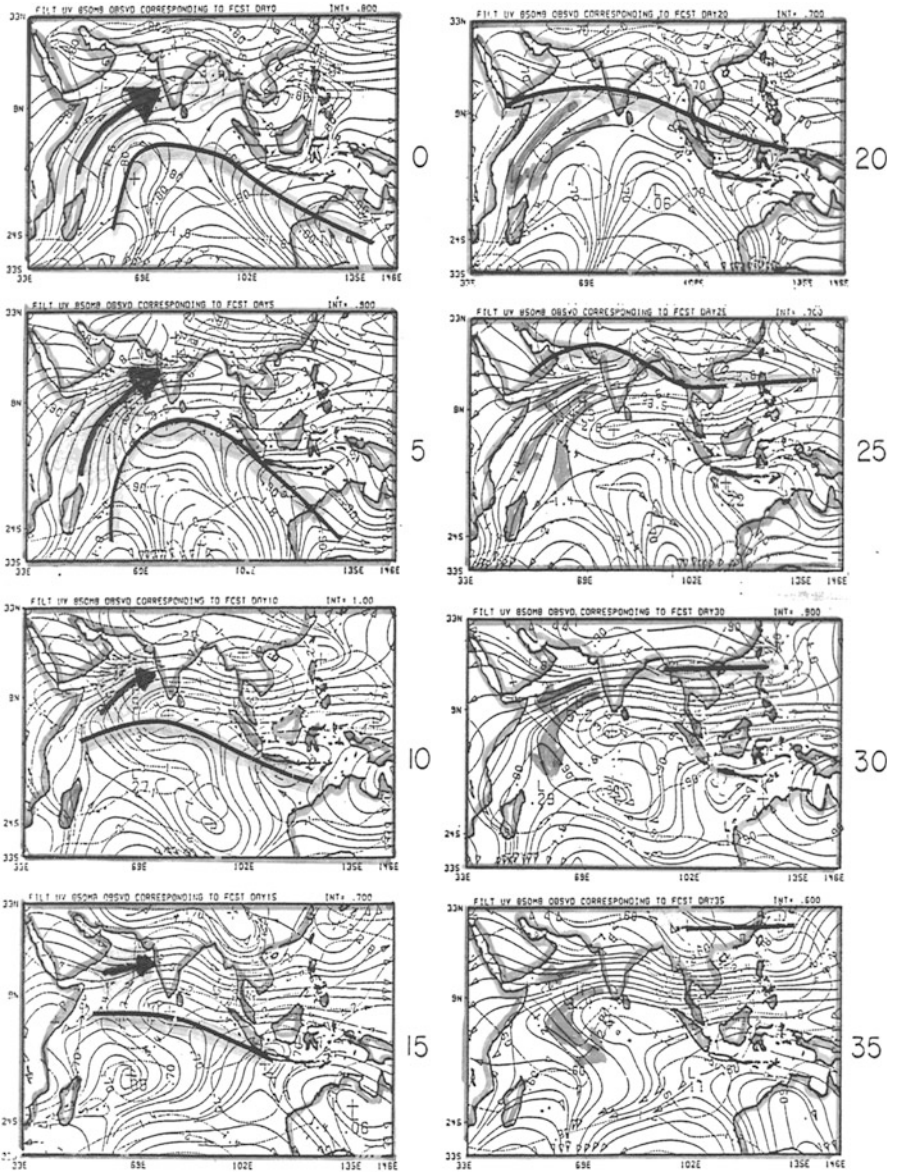

Fig. 7.6 A sequence of 950 mb observed flow fields (time filtered on the scale of 30–50 days) for the experiment on dry spell over India. Streamlines (*solid lines*) and isotachs (*dashed lines*) are shown here. Units of ms^{-1}

an emanating component of a weaker ISO wave moving southwards from the southern equatorial trough. This feature is not well understood at the present time. The modulation of weather during the monsoon months from the northward moving component of the ISO wave has been well documented.

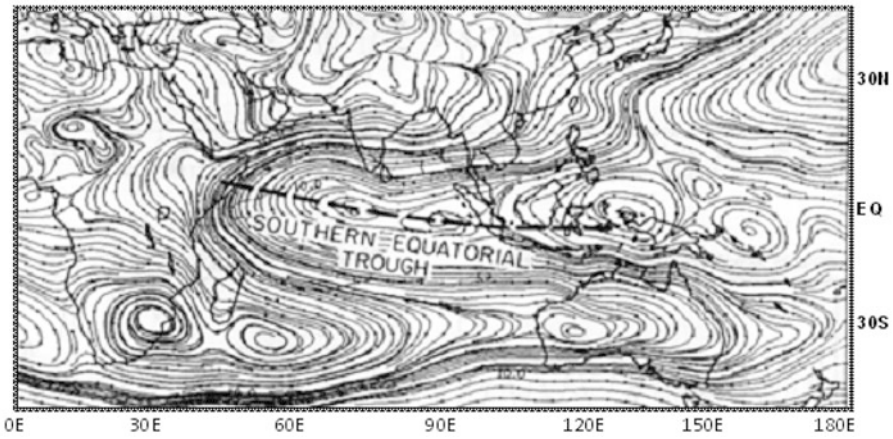

Fig. 7.7 Climatology of the 850 mb streamlines based on FGGE data set for July 1979. The southern equatorial trough is emphasized here as a source region for the meridionally propagating low frequency waves (After Krishnamurti et al. 1992b)

7.2 Theory of the MJO

Lau and Peng (1987) presented a theory for those eastward propagating Madden Julian waves that traverse around the earth in roughly 40 days. This theory states that these waves undergo an interaction with convection that can be studied by a mechanism called wave CISK. This being a promising theory, we present an outline of it here.

In their analysis Lau and Peng (1987) make use of a global model that is described by the following vorticity and divergence equations, the mass continuity equation, the first laws of thermodynamics and the hydrostatic law. This constitutes a closed system of five equations for the vorticity, divergence, temperature, surface pressure, and the geopotential height. In a σ-coordinate system these are:

$$\frac{\partial \zeta}{\partial t} = -\nabla \cdot (\zeta + f)\vec{\mathbf{V}} - \vec{\mathbf{k}} \cdot \nabla \times \left(RT\nabla q + \dot{\sigma}\frac{\partial \vec{\mathbf{V}}}{\partial \sigma} - \vec{\mathbf{F}} \right) \tag{7.2}$$

$$\frac{\partial D}{\partial t} = -\vec{\mathbf{k}} \cdot \nabla \times (\zeta + f)\vec{\mathbf{V}} - \nabla \cdot \left(RT\nabla q + \dot{\sigma}\frac{\partial \vec{\mathbf{V}}}{\partial \sigma} - \vec{\mathbf{F}} \right) - \nabla^2 \left(\phi + \frac{\vec{\mathbf{V}} \cdot \vec{\mathbf{V}}}{2} \right) \tag{7.3}$$

$$\frac{\partial T}{\partial t} = -\nabla \cdot T\vec{\mathbf{V}} + TD + \dot{\sigma}\gamma - \frac{RT}{C_p}\left(D + \frac{\partial \dot{\sigma}}{\partial \sigma} \right) + H_T \tag{7.4}$$

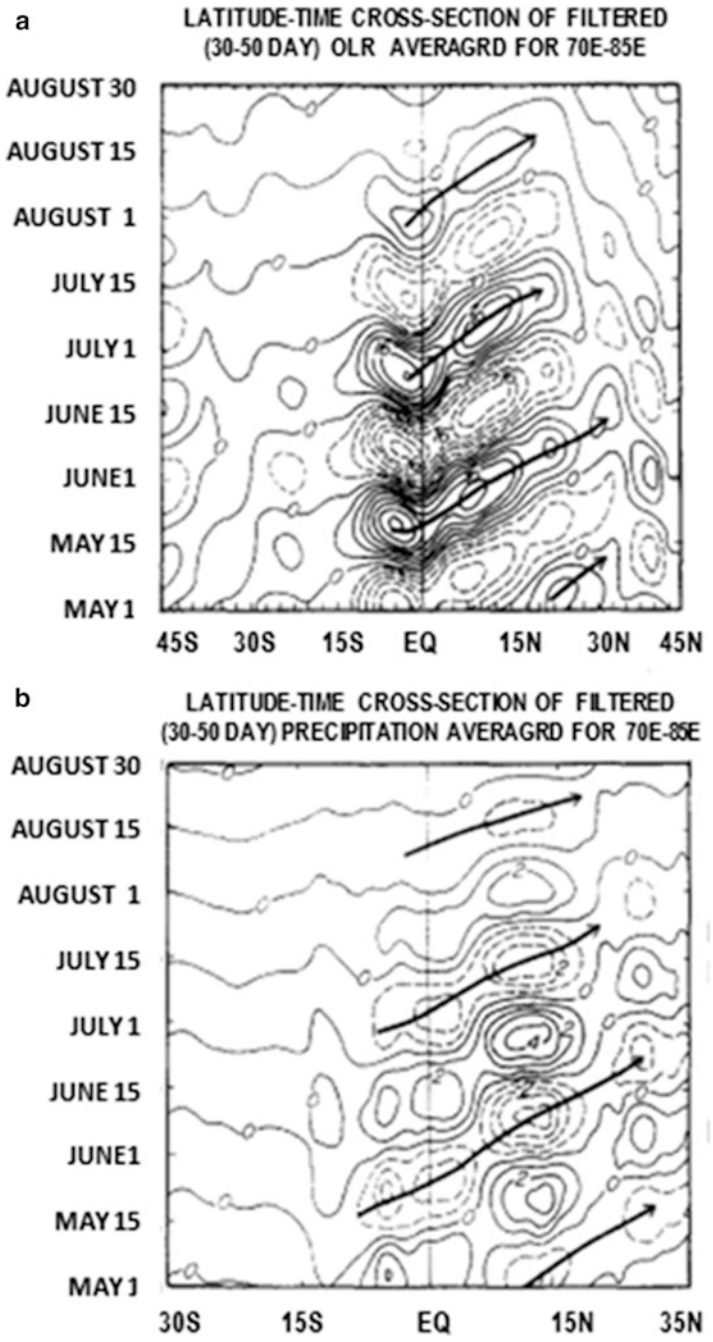

Fig. 7.8 Latitude-time cross-section of 30–50 days time filtered (**a**) u wind (ms^{-1}) and (**b**) vorticity (s^{-1}) at 850 mb (After Krishnamurti et al. 1997)

$$\frac{\partial q}{\partial t} = -\vec{\mathbf{V}} \cdot \nabla q - D - \frac{\partial \dot{\sigma}}{\partial \sigma} \tag{7.5}$$

$$\sigma \frac{\partial \phi}{\partial \sigma} = -RT, \tag{7.6}$$

where ζ is the vorticity, D is the divergence, $\vec{\mathbf{V}}$ is the horizontal wind vector, T is the temperature, $q = \ln p_s$, i.e., the logarithm of the surface pressure, $\gamma = RT/c_p\sigma - \partial T/\partial\sigma$ is the static stability parameter, $\vec{\mathbf{F}}$ is the frictional force, and H_T represents the diabatic heat sources and sinks.

The model used by Lau and Peng (1987) was a standard global spectral model that was run at a resolution of 15 wave (Rhomboidal Truncation), with five levels in the vertical. The global spectral model is a forecast model which carries certain physical parameterization models; see any standard text (e.g. Krishnamurti et al. 2006) for details on such modeling. In their work Lau and Peng (1987)included the following features in their global spectral model:

1. Rayleigh friction for dissipation. This is of the form $-K\zeta$ in the vorticity equation and $-KD$ in the divergence equation.
2. Newtonian Cooling of the form $-KT$ as proxy for net radiative cooling in the thermal equation of the first law of thermodynamics.
3. No surface topography.
4. Convective heating is the only form of diabatic heating that is included.

They introduce a conditional convective heating defined by the equation:

$$Q(\sigma) = \begin{cases} -m\eta(\sigma) r L q_{sat}(T_5) D_5 \Delta\sigma / C_p & D_5 < 0 \\ 0 & D_5 \geq 0 \end{cases} \tag{7.7}$$

This heating Q is defined on sigma surfaces. The relationship between this Q and H_T in (7.4) is given by $H_T = \frac{1}{C_p}\frac{\theta}{T}Q$. D_5 is the divergence at the lowest model level (level 5) which is at the $\sigma = 0.9$ surface i.e. close to 900 mb level. r is the prevailing relative humidity at the $\sigma = 0.75$ surface (roughly 750 mb level). Only level convergence influences the heating (there is no cooling mechanisms here). q_{sat} is the saturation specific humidity at the temperature T_5 at the $\sigma = 0.90$ level. $\eta(\sigma)$ is a normalized vertical profile of heating (whose vertical integral is 1).

The conditional instability of the first kind refers to the growth of small perturbations in a conditionally unstable atmosphere. This is based on a linear analysis that was carried out by Kuo (1961) and Lilly (1960). They noted that the most unstable (i.e. the most amplifying) mode in such an atmosphere was on the cloud scale of the order of few km. Since tropical disturbances on the scale on the order of 3,000 km abound in the tropics (such as easterly waves) Charney and Eliassen (1964) proposed a theory for shifting the scale of instability from few kilometers to several 1,000 km scale. This is known as the conditional instability of the second kind, or CISK. This requires, mathematically, that the heating be

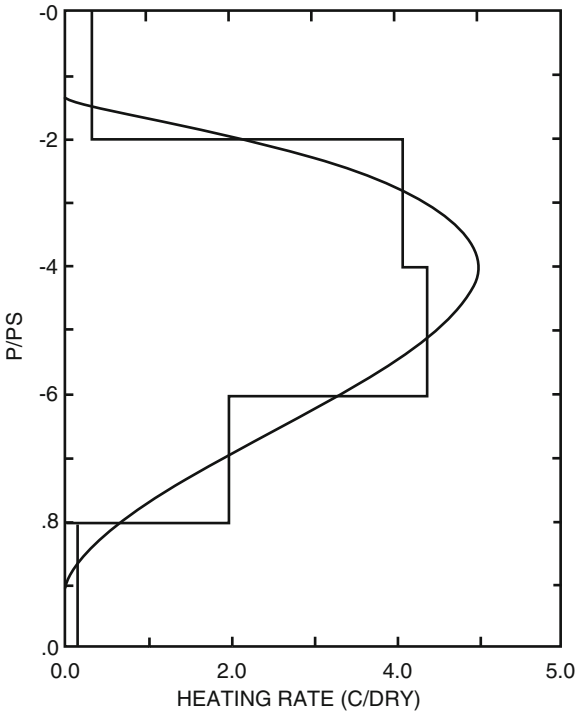

Fig. 7.9 Vertical structure of heating profile (Adopted from Lau and Peng 1987). Actual values used in the model layer are shown as discrete *solid lines*. Units in $^{\circ}$C day^{-1}

independent of the internal vertical velocity of the growing perturbations. The analysis of the growth of linear perturbations, in a conditionally unstable atmosphere, with heating proportional to the Ekman pumping (vertical velocity) at the top of the boundary layer shows that the growth rates are indeed on scales much larger than the cloud scales.

The CISK produced by the internal waves such as gravity, Kelvin, mixed gravity Rossby and Rossby waves in the absence of any explicit Ekman pumping is defined as wave CISK (Lindzen 1974). In the CISK mechanism, low level convergence is provided by the passing of lower tropospheric waves, the effectiveness of Ekman pumping close to the equator seems dubious. Internal waves are highly convergent and need no Ekman pumping to produce CISK. The latent heat release processes are case dependent and are similar to those of CISK.

Figure 7.9 shows the vertical structure of the internal heating in this five-layer model. At every grid point that encounters mass convergence, $D_5 < 0$, the vertical structure given by $\eta(\sigma)$ is imposed following (7.7) which dictates the amplitude of the overall heating. The initial horizontal structure of the external heating is described in Fig. 7.10. This is a zonally asymmetric dipole of heating (solid lines) and cooling (dashed lines). This is initially inserted as an external forcing and after a model spin up that takes about 5 days, the external heating is removed and from an internal heating that moves with the Kelvin wave. The time longitude section of the 300 mb zonal wind (ms^{-1}) along the equator is shown in Fig. 7.11. This clearly

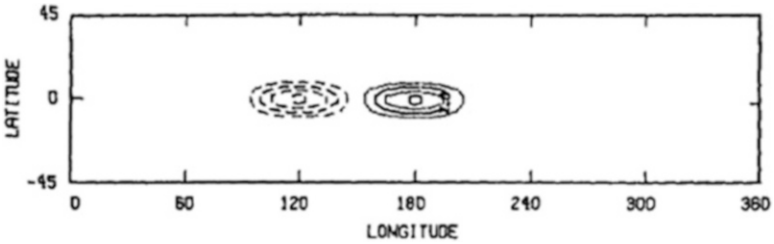

Fig. 7.10 Spatial structure of the oscillating dipole heat source with a 44-day period at Day 77 when positive (negative) heating is strongest over 180° (120°) longitude. Contour starts at 1°C for every 2°C (After Lau and Peng 1987)

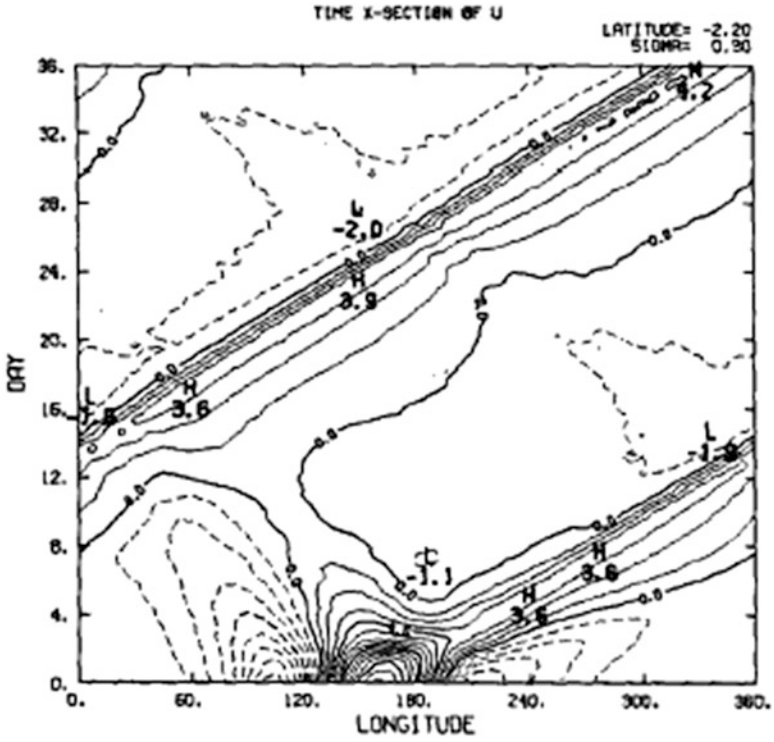

Fig. 7.11 Time longitude section of 300 mb zonal wind (ms^{-1}) from an idealized experiment where CISK like heating is prescribed (After Lau and Peng 1987)

shows the zonal propagation of the zonal wind anomalies that carry an amplitude of roughly 3–4 ms^{-1} which is close to the observed values. This illustration also shows the initial spin up period of roughly 5 days that was imposed. Strong westerlies and weak easterlies propagate eastward around the globe in roughly 25 days. This wave is driven by the free dynamics of the Kelvin waves plus the forced dynamics from the wave CISK. The march of precipitation follows a similar cycle that is shown in

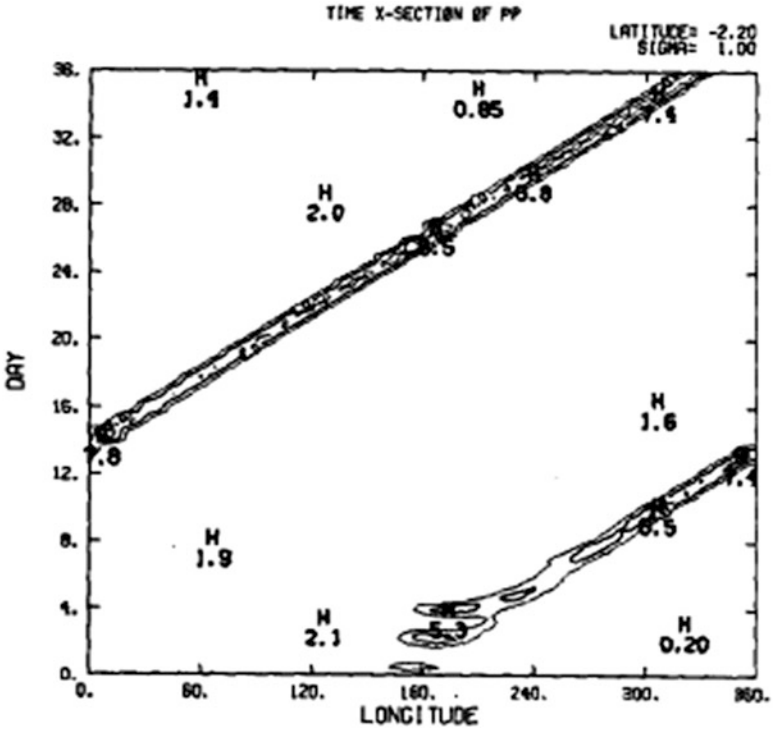

Fig. 7.12 Same as Fig. 7.11 but for precipitation (mm day^{-1}) (After Lau and Peng 1987)

Fig. 7.12. This was a successful theory and modeling effort for Lau and Peng (1987). Their essential finding could be summarized by stating that one needs a simple wave CISK (i.e. heating proportional to the surface convergence of traversing waves) to model the eastward propagating MJO phenomenon. The waves in question here are long planetary waves (wave numbers 1 and 2). The amplitudes of wind perturbations were reasonably modeled. The phase speed of the eastward propagating MJO of roughly 20 ms^{-1} in this experiment was twice what is observed. Lau and Peng (1987) attribute that difference to the slowing down effects of more realistic ocean atmosphere coupling and imply the need for modeling of super cloud clusters.

Wave CISK is normally applied to synoptic scale tropical waves with wavelengths on the order of few 1,000 km. This application of wave CISK on scales on the order of 10,000 km for planetary scale Kelvin waves is clearly open to question since this requires a modulation of convection by convergence on the scale of this planetary wave. It is more likely that a number of smaller scale waves and smaller scale convection is organized on the scale of MJO. Those were not resolved by the simple model configuration of Lau and Peng (1987). A richer spectrum of scales is seen in more recent modeling studies of the MJO.

Randall et al. (2003) proposed that the modeling of the MJO would require the modeling of the deep convective elements that form a super cloud cluster. Towards this end they designed a global model (with prescribed monthly mean ocean temperatures) that carried explicit clouds. In such a model they were able to replicate many features of the MJO.

Other scientists, such as Saha et al. (2006) point out that a coupled atmosphere ocean model is necessary for the simulation of MJO since that time scale is present in the SST anomaly fields.

7.3 Westerly Wind Bursts in the MJO

The MJO signal in the zonal wind is fairly robust. Surface and 850 mb winds have been examined in a number of studies and it has been noted that in the equatorial latitudes the westerly phase of the MJO is often accompanied by strong wind surges. This signature is sufficiently strong that it is also seen in the total zonal wind i.e. the total wind (not just the wind anomaly) is also westerly in the equatorial latitudes. This is observed in the Indian Ocean and the western Pacific Ocean. A westerly wind burst in the equatorial latitudes creates a cyclonic shear of the horizontal wind in both hemispheres across this wind belt. Often in these regions of strong cyclonic shear vortices form that eventually become tropical depressions leading to tropical cyclones (or typhoons). A spectacular example of such an event is shown in Fig. 7.13 where two pairs of tropical cyclones have formed on either side of the equator – one over the Arabian Sea/Indian Ocean and the other over the Bay of Bengal/Indian Ocean. This event occurred during May 2003. The 850 mb winds of the westerly wind burst in the equatorial latitudes was on the order of 15 ms^{-1}.

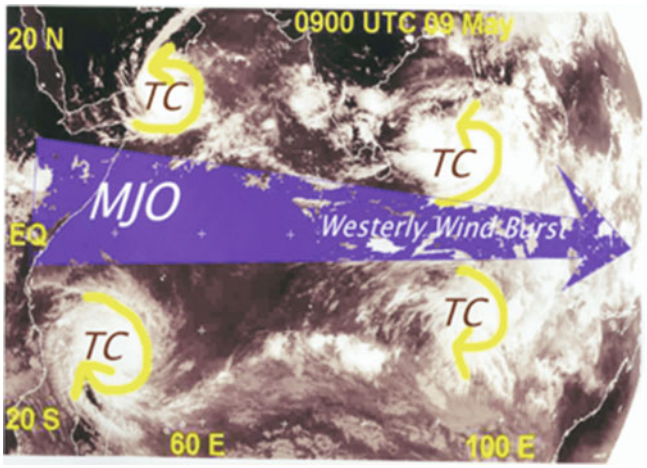

Fig. 7.13 Two pairs of tropical cyclones during a westerly wind burst seen on May 9, 2003

7.4 The MJO Connection During the Birth and Demise of ENSO

Considerable observational evidence has accumulated to show that some westerly phases of the MJO extend eastwards into the Pacific Ocean in the formative stages of an El Nino event. This is illustrated in Fig. 7.14 from Krishnamurti et al. (2000). These are Hovmöller diagrams (longitude/time) averaged over the equatorial belt 5°S to 5°N of the daily zonal wind at the 850 mb level. The westerly wind anomalies at the MJO time scale are shaded. Rectangular boxes indicate the period of El Nino onset. These tend to coincide with the periods during which there is a marked eastward propagation of the westerly MJO-scale anomalies. The periods when the westerly wind phases of the MJO extend into the Pacific Ocean seem to coincide with the onset of El Nino for the years 1968–69, 1971–72, 1976, 1981–82, 1991–92, 1992–93, and 1996–97. That aspect of the weakening of the lower tropospheric easterlies originating in the Indian Ocean was also illustrated in Chap. 4, Sect. 4.3 and Fig. 4.4. This appears to be an important antecedent feature of the El Nino in most years.

There is also some evidence of the role of MJO activity on the in the equatorial Indian Ocean playing a role in the termination of El Nino events. Takayabu et al. (1999) reported on the termination of the El Nino of the 1997/98 season. They examined equatorial Hovmöller diagrams for precipitation, sea surface temperatures and surface winds and found a strong MJO with a strong easterly phase propagating into the Pacific Ocean. This event coincided with the abrupt termination of the El Nino of the 1997–98 (cf Fig. 7.2 in Takayabu et al. 1999). In the second half of May 1998 the sea surface temperatures cooled to below 27°C at around 120°W over the eastern Pacific Ocean. This highlighted the end of the warm phase of the 1997–98 El Nino. The other notable feature of that figure is the strong easterlies representing a build-up of the Pacific trades. During May of 1998 the propagation of strong easterly winds from the Indian Ocean to the equatorial Pacific Ocean (3°S to 3°N) is clearly evident.

7.5 Wave Energy Flux Across the Tropics

The linear theories of Eliassen and Palm (1961) and later by Yanai and Lu (1983) provide the following equation to describe the wave energy flux across a latitude circle:

$$\overline{\phi' v'} = (\bar{u} - c)\left[\overline{u'v'} - \frac{1}{\sigma_o}\frac{\overline{\partial u}}{\partial p}\frac{\overline{v'\partial \phi'}}{\partial p}\right]$$

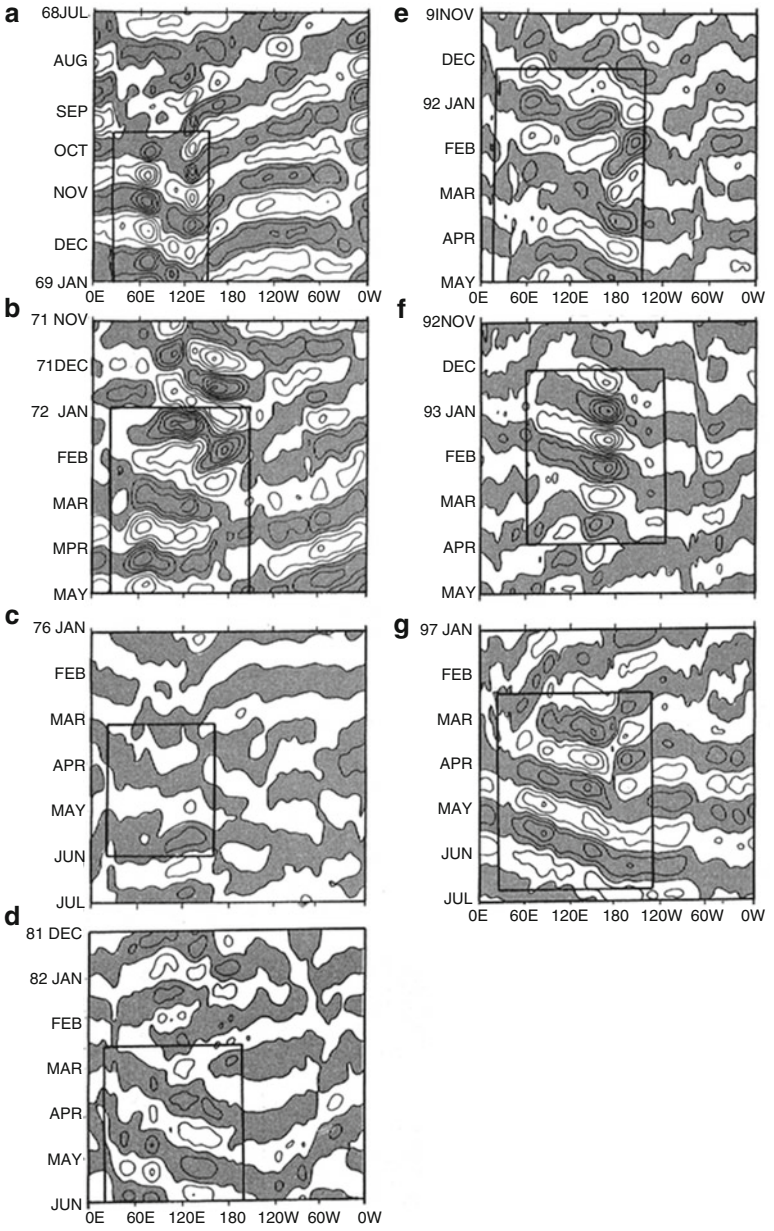

Fig. 7.14 Longitude–time sections of the time-filtered (30–60 days) zonal winds at 850 mb. Shaded areas denote westerly anomalies. Results for different El Niño years ((**a**) 1968–69, (**b**) 1971–72, (**c**) 1976, (**d**) 1981–82, (**e**) 1991–92, (**f**) 1992–93, and (**g**) 1996–97). *Boxes* indicate the time of El Nino onset (After Krishnamurti et al. 2000)

Here $\phi' v'$ denotes the wave energy flux across a latitude circle; $\bar{u}$ is the zonally averaged zonal wind; c is the phase speed of the wave; $u'v'$ denotes the meridional eddy flux of momentum; σ_o is a reference dry static stability; $\overline{\frac{\partial u}{\partial p}}$ denotes the vertical shear of the zonally averaged zonal wind; $\overline{\frac{v' \partial \phi'}{\partial p}}$ is a measure of the meridional heat flux across a latitude circle.

It is clear that when u-c goes to zero the wave energy flux vanishes. Thus a major conclusion was drawn that this latitude where u-c vanishes is a critical latitude and a barrier that does not permit any wave energy exchange from tropics to middle latitudes to occur and vice versa. That means that tropical wave activity cannot influence the higher latitudes, nor can the extratropical wave activity directly influence the tropics across such a barrier. This was an accepted result in many subsequent studies. There is however a major flaw in this linear theory. Almost all scales of motion including the zonally averaged flows carry temporal variabilities on many time scales. Those include variabilities in biennial, annual, MJO, ENSO and decadal time scales. The nature of this problem changes as soon as we include the presence of such other time scales. That becomes a problem of wave energy flux in the frequency domain, Krishnamurti et al. (1997). In that formulation $\bar{u}$ is no more a constant, nor are other time averaged terms. Nonlinearity is present in such a formulation in the starting equations from which the wave energy fluxes are derived. We shall not present a derivation of that equation here, except to state that it is possible to write an expression for $\overline{\phi' v'}$ that includes many more terms. Those terms arise from the complete dynamical and the thermodynamical equations including all of the non linear advective terms. Given reanalysis data sets, in principle, one can compute such wave energy fluxes. One then asks the question does the wave energy flux still vanish or is it near zero around the critical latitudes of the linear problem. Computations of such quantities do suggest that the total wave energy flux across the liner theory based critical latitudes are indeed very small. This might suggest that the linear theory is being confirmed from the inclusion of non linear terms of the complete equations. However one can take a further step with these equations. These complete wave energy flux equations can be cast in a frequency domain and one can ask what are the fluxes within certain windows of time scales. One such question is what goes on at the MJO time scale. That question was addressed by Krishnamurti et al. 1997. They found that the critical latitude is not a barrier in the frequency domain, large amounts of wave energy flux escapes from the tropics to the higher latitudes across the barrier since $\bar{u}$ is not a constant but has a temporal variability on the MJO time scale. At higher frequencies, on the other hand, wave energy flux returns to the tropics from the extratropics. Although the total wave energy flux, summed over all frequency windows is small, there is a large communication between the tropics and the higher latitudes at individual frequencies. In that light the MJO time scale is very interesting since it sees a substantial exchange of energy between the tropics and the middle latitudes.

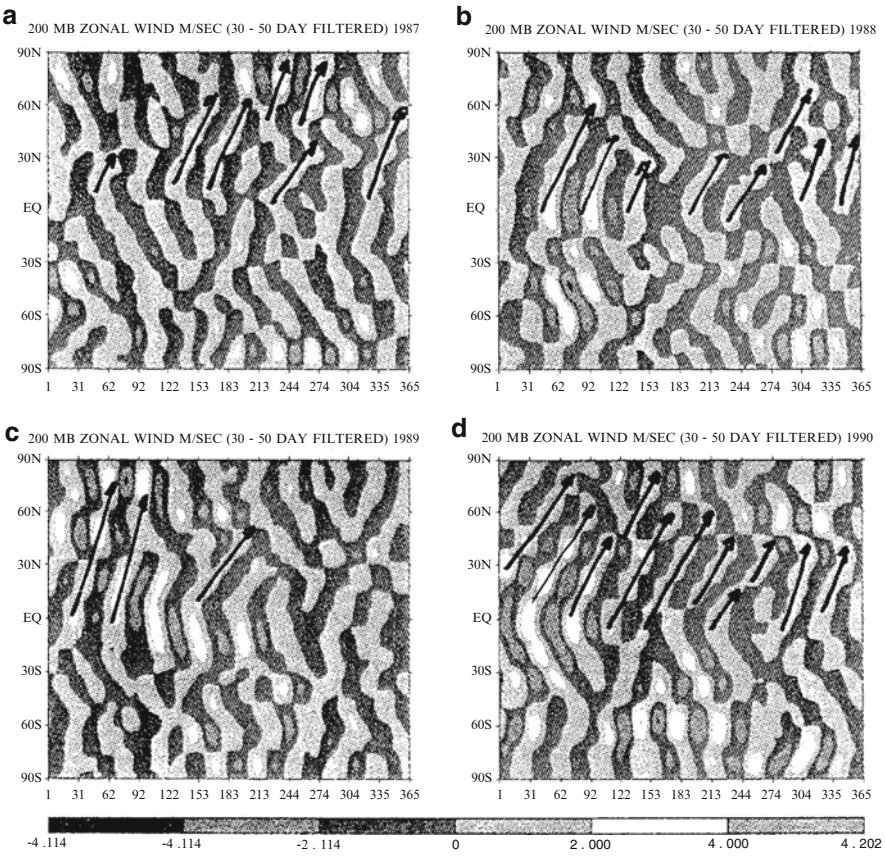

Fig. 7.15 Latitude-time diagram of meridional wave energy flux $\overline{\phi' v'}$ on the time scale of 30–50 days. Four separate years of result are shown for the years (**a**) 1987, (**b**) 1988, (**c**) 1989, and (**d**) 1990 here. The ordinate denotes latitude, the abscissa denotes day of the year. Units are Jms^{-1}

An illustration of wave energy flux as a function of latitude and time in days is shown in Fig. 7.15. This is a vertical integral of the wave energy flux through the troposphere and is zonally averaged. What we see here is a substantial meridional propagation of wave energy flux from the tropics to the higher latitudes. The latitude belt 30–60 N latitudes show a rightward slope for these fluxes, meaning a northward flux as a function of time. It also suggests a strong convergence of wave energy flux near 60 N. There exists a large variance for the zonal wind anomalies on the time scale of 30–60 days, (the MJO time scale) at around 60 N latitude. The linear theory fails to connect the tropical signals on the MJO time scale with those of the higher latitudes. The selective fluxes across the critical latitude are possible in the frequency domain, making it possible to have a communication between the tropics and the higher latitudes.

7.6 Real Data Forecasts of ISO

In a series of modeling experiments Krishnamurti et al. (1990, 1992b, 1995) showed that it is possible to predict at least one cycle of the passage of an ISO wave of the Indian, the Chinese and the Australian Monsoon. The premise of these studies is based on the fact that the superposition of the intraseasonal circulation anomalies and the climatological circulations favors enhanced or deficient rainfall anomalies. This is illustrated schematically in Figs. 7.16, 7.17, and 7.18 for the Indian, the Chinese and the Australian components of the monsoon respectively.

In the case of the Indian monsoon, the climatological southwesterly flow is weakened by the transients (intraseasonal component; Fig. 7.16a, b) resulting in the dry spell of the monsoon. Likewise during the wet spell of the Indian monsoon the southwesterly flow is enhanced by the intra-seasonal component (Fig. 7.16c, d) of the low level flow. Similarly the modulation of the climatological West Pacific subtropical high by the intra-seasonal component of the low level flow (~850 mb) leads to the wet and dry spells of the Chinese monsoon (Fig. 7.17). In the context of the Australian monsoon it is the modulation of the inter-tropical convergence zone in between 10 and 15 S that undergoes modulation from the passage of the intraseasonal modes as illustrated in Fig. 7.18.

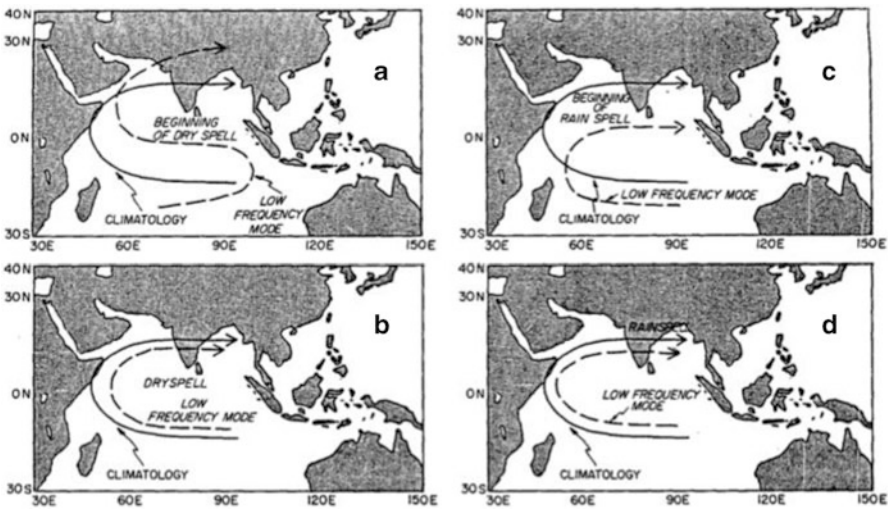

Fig. 7.16 Schematic pictures of (**a**, **b**) anti-parallel and (**c**, **d**) parallel flows that produce anomalous dry and wet periods of the Indian monsoon (After Krishnamurti et al. 1992b)

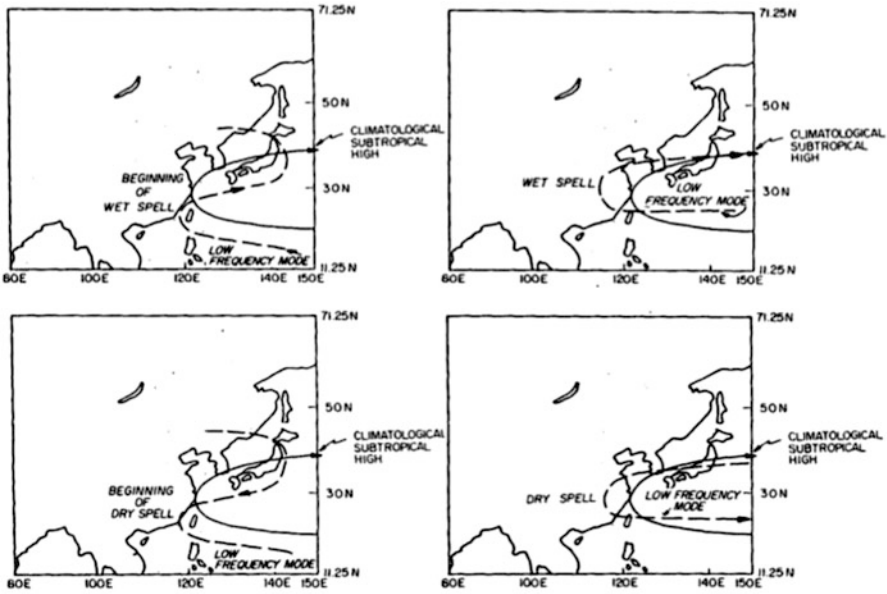

Fig. 7.17 Same as Fig. 7.16 but for the Chinese monsoon (After Krishnamurti et al. 1992b)

Krishnamurti et al. (1990, 1992b, 1995) proposed an initialization technique for an atmospheric model that could predict one cycle of this intra-seasonal mode. This intialization technique was based on the fact that the growth of the very high frequency variability during the integration of the model contaminated the forecasts of the intra-seasonal modes. Furthermore, it was felt that the SST carries an anomaly on the timescale of the ISO, which follows from an earlier observational study (Krishnamurti et al. 1988). Therefore, a low band pass filter was used on the SST to retain the intra-seasonal modes from the past 120 days prior to day 0 (or start) of the forecast at every ocean grid point of the model. These anomalies were then simply extrapolated into the future preserving their recent past amplitudes. However its phase was varied based on extrapolation of the past cycle that was obtained from the observed SST. Likewise all the all the atmospheric variables were also low pass filtered and only the low frequency anomalies were retained at day zero of the forecast. Figure 7.19a, b show the typical error growth for a month from such an initialized forecast for 850 mb winds for the globe and for the Asian monsoon region. In these forecasts the anomaly correlation was over 0.5 at day 30 of the forecast.

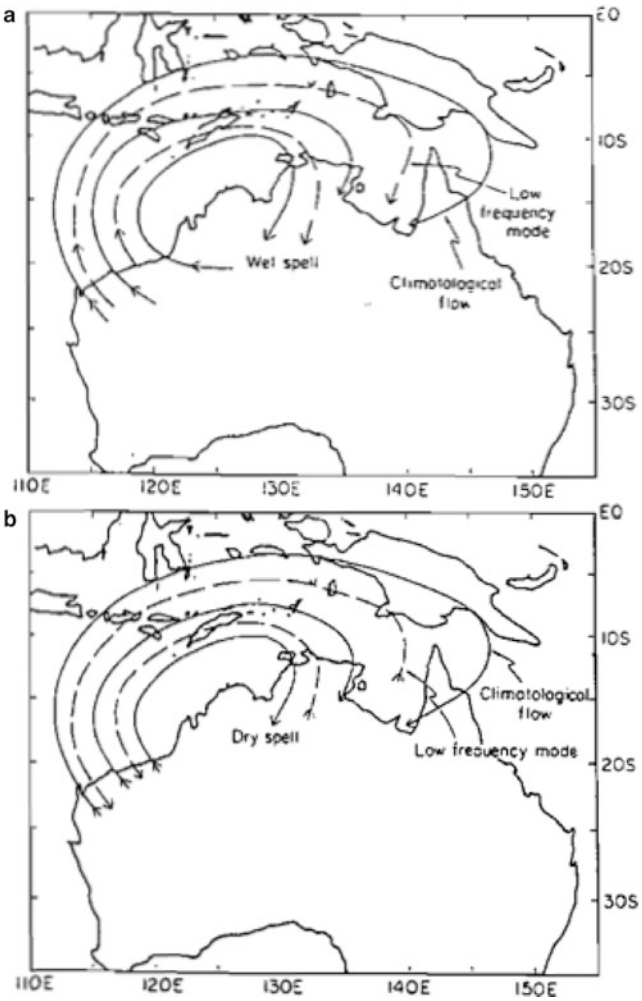

Fig. 7.18 Schematic illustration of the (**a**) parallel and (**b**) anti-parallel flow that produces wet and dry spells of the Australian monsoon (After Krishnamurti et al. 1995)

The full forecast of the 850 hPa winds (time filtered on the scale of 30–60 days) is displayed in Fig. 7.20 at 5 day intervals. For comparison the corresponding observations are shown in Fig. 7.21. The predicted ISO waves in Fig. 7.20 show a remarkable agreement during the first phase of the ISO with the corresponding observations in Fig. 7.21, suggesting that this method of removing high frequencies initially and including an oceanic forcing can provide a prediction of the ISO.

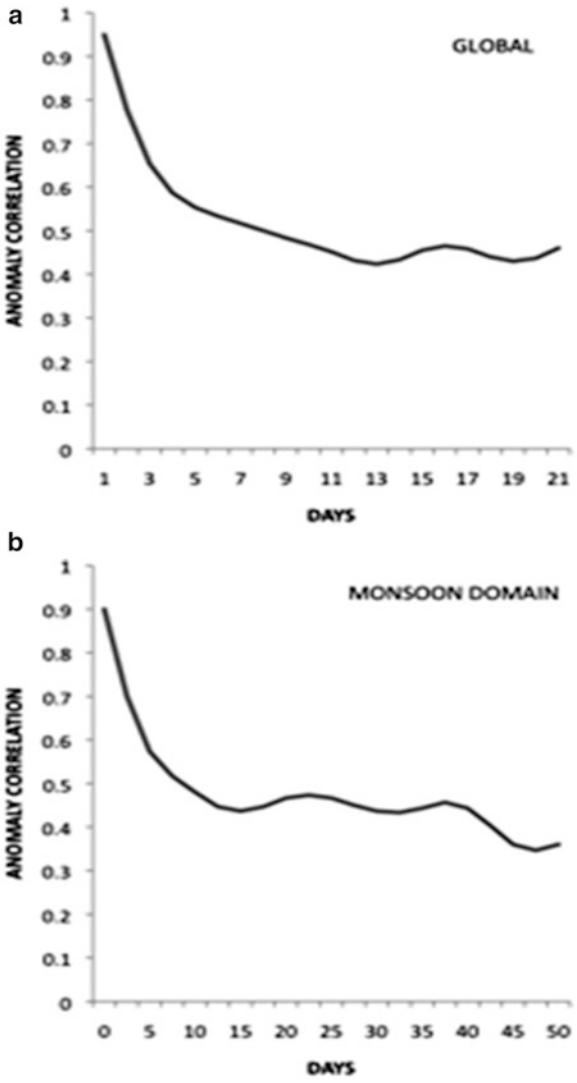

Fig. 7.19 Anomaly correlation of 850 mb winds for (**a**) global and (**b**) monsoon domain from the intialization experiments for low frequency variability forecasts (After Krishnamurti et al. 1992b)

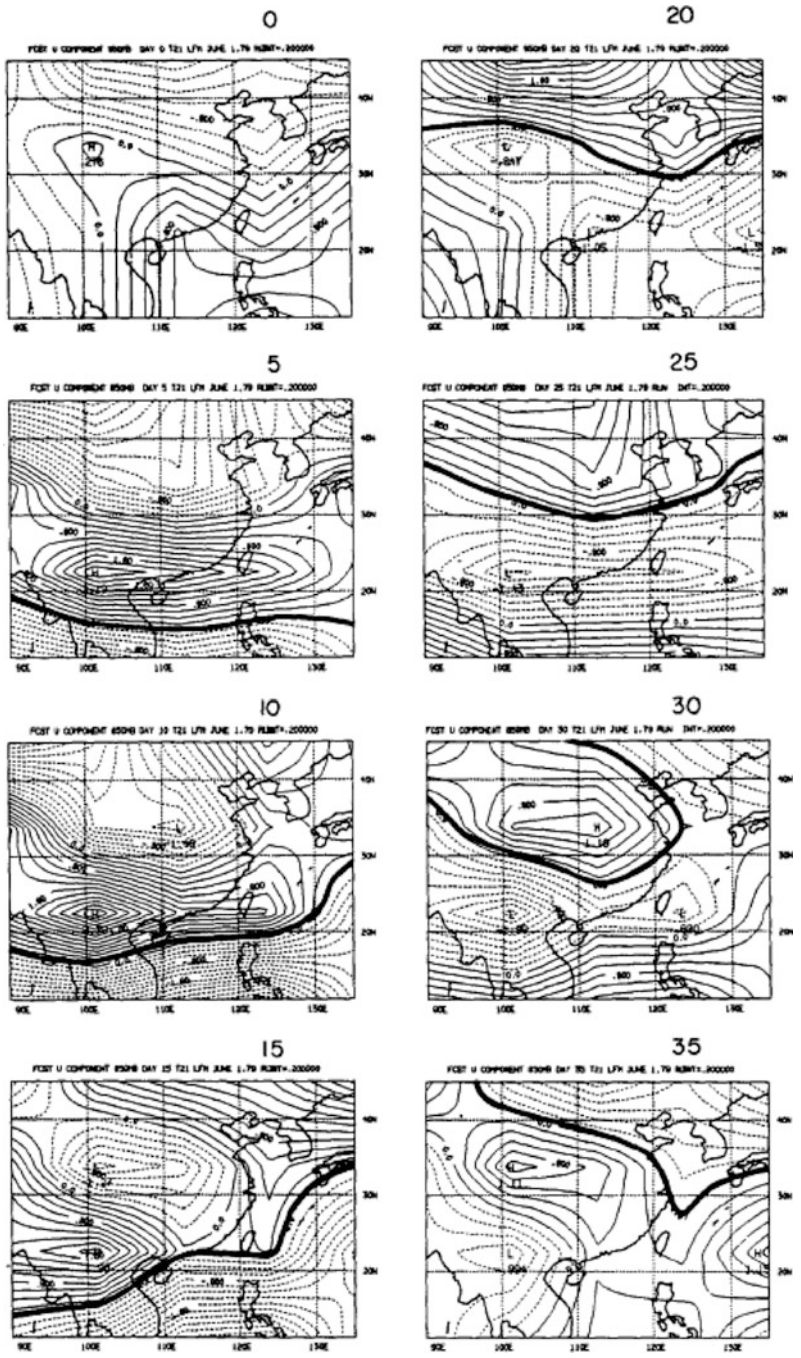

Fig. 7.20 Panels of the 850 mb zonal winds (ms^{-1}) based on the intraseasonal forecasts. Day 0 is June 1, 1979. Maps are shown at intervals of 5 days (After Krishanmurti et al. 1992b)

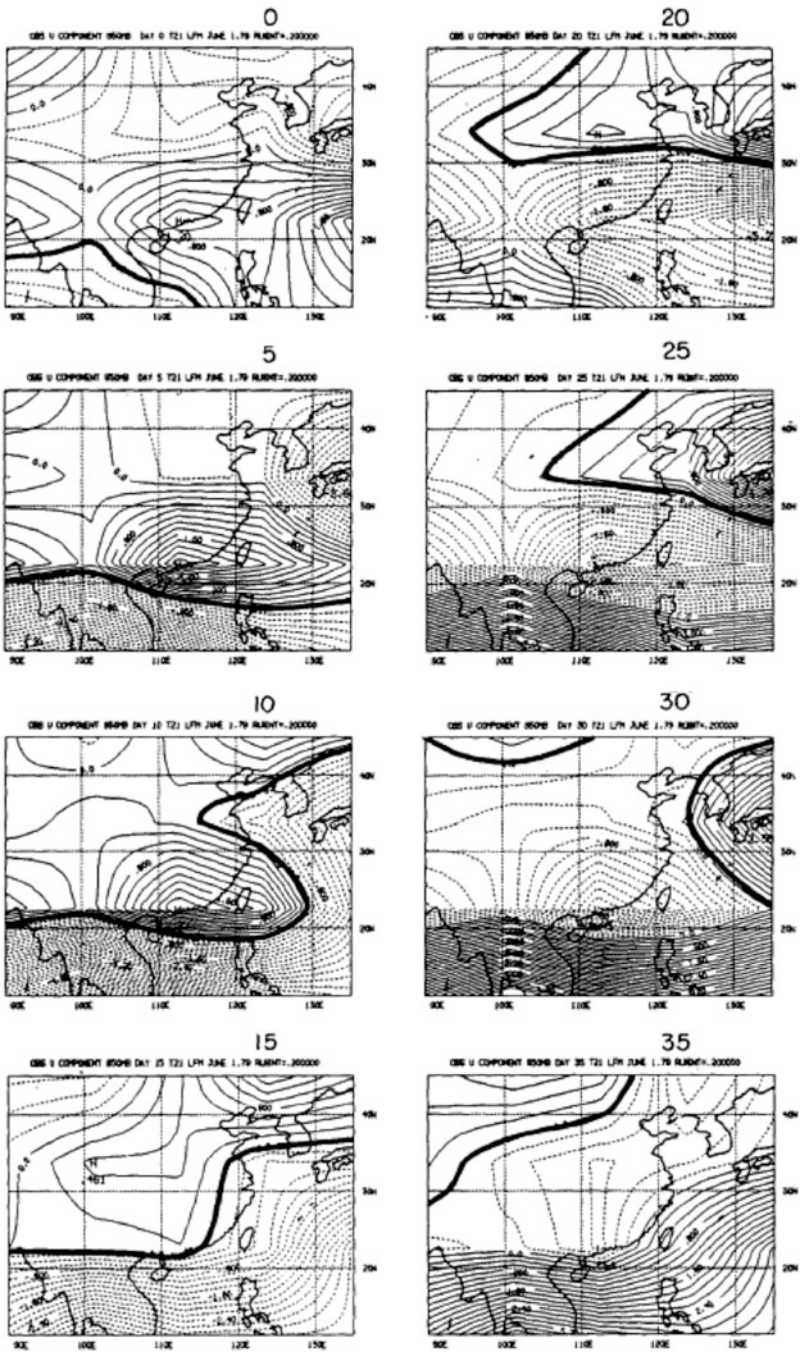

Fig. 7.21 Same as Fig. 7.20 but from observations (ECMWF'S FGGE analysis for MONEX year 1979) (After Krishanmurti et al. 1992b)

References

Charney, J., Eliassen, A.: On the growth of the hurricane depression. J. Atmos. Sci. **21**, 68–75 (1964)
Eliassen, A., Palm, E.: On the transfer of energy in stationary mountain waves. Geof. Pub. **3**, 1–23 (1961)
Krishnamurti, T.N., Jayakumar, P.K., Sheng, J., Surgi, N., Kumar, A.: Divergent circulations on the 30–50-day time scale. J. Atmos. Sci. **42**, 364–375 (1985)
Krishnamurti, T.N., Oosterhof, D., Mehta, A.V.: Air-sea interaction on the time scale of 30–50 days. J. Atmos. Sci. **45**, 1304–1322 (1988)
Krishnamurti, T.N., Subramaniam, M., Oosterhof, D., Daughenbaugh, G.: On the predictability of low frequency modes. Meteorol. Atmos. Phys. **44**, 131–166 (1990)
Krishnamurti, T.N., Sinha, M.C., Krishnamurti, R., Oosterhof, D., Comeaux, J.: Angular momentum, length of day, and monsoonal low frequency mode. J. Meteorol. Soc. Jpn. **70**(1B), 131–166 (1992a)
Krishnamurti, T.N., Subramaniam, M., Daughenbaugh, G., Oosterhof, D., Xue, J.: One month forecasts of wet and dry spells of the monsoon. Mon. Weather Rev. **120**, 1191–1223 (1992b)
Krishnamurti, T.N., Han, S.–.O., Misra, V.: Prediction of wet and dry spells of the Australian Monsoon. Int. J. Climatol. **15**, 753–771 (1995)
Krishnamurti, T.N., Sinha, M.C., Misra, V., Sharma, O.P.: Tropical-middle latitude interactions viewed via wave energy flux in the frequency domain. Dyn. Atmos. Oceans **27**(1997), 383–412 (1997)
Krishnamurti, T.N., Bachiochi, D., LaRow, T., Jha, B., Tewari, M., Chakraborty, D.R., Correa-Torres, R., Oosterhof, D.: Coupled atmosphere–ocean modeling of the El Niño of 1997–98. J. Climate **13**, 2428–2459 (2000)
Krishnamurti, T.N., Bedi, H., Hardiker, V., Ramaswamy, L.: An Introduction to Global Spectral Modeling. Springer, 317pp. 2nd, rev. and enlarged ed (2006)
Kuo, H.L.: Convection in conditionally unstable atmosphere. Tellus **13**, 441–459 (1961)
Lau, K.M., Peng, L.: Origin of low-frequency (intraseasonal) oscillations in the tropical atmosphere. Part I: The basic theory. J. Atmos. Sci. **44**, 950–972 (1987)
Lilly, D.K.: On the theory of disturbances in a conditionally unstable atmosphere. Mon. Weather Rev. **88**, 1–17 (1960)
Lindzen, R.S.: Wave-CISK in the tropics. J. Atmos. Sci. **31**, 156–179 (1974)
Madden, R.A., Julian, P.R.: Detection of a 40–50 day oscillation in the zonal wind in the tropical Pacific. J. Atmos. Sci. **28**, 702–708 (1971)
Nakazawa, T.: Tropical super clusters within intraseasonal variations over the western Pacific. J. Meteorol. Soc. Jpn. **66**, 823–839 (1988)
Randall, D., Khairoutdinov, M., Arakawa, A., Grabowski, W.: Breaking the cloud parameterization deadlock. Bull. Am. Meteorol. Soc. **84**(11), 1547–1564 (2003)
Saha, S., et al.: The NCEP climate forecast system. J. Climate **19**, 3483–3517 (2006)
Takayabu, Y.N., Iguchi, T., Kachi, M., Shibata, A., Kanzawa, H.: Abrupt termination of the 1997–98 El Nino in response to a Madden-Julian oscillation. Nature **402**, 279–282 (1999)
Yanai, M., Lu, M.–.M.: Equatorially trapped waves at the 200 mb level and their association with convergence of wave energy flux. J. Atmos. Sci. **40**, 2785–2803 (1983)